THE JOURNAL OF PHYSICAL CHEMISTRY Letters

Letter

pubs.acs.org/JPCL

Self-Assembly of Flux-Closure Polygons from Magnetite Nanocubes

Megan W. Szyndler and Robert M. Corn*

Department of Chemistry, University of California—Irvine, Irvine, California 92697, United States

Supporting Information

ABSTRACT: Well-defined nanoscale flux-closure polygons (nanogons) have been fabricated on hydrophilic surfaces from the face-to-face self-assembly of magnetite nanocubes. Uniform ferrimagnetic magnetite nanocubes (~86 nm) were synthesized and characterized with a combination of electron microscopy, diffraction, and magnetization measurements. The nanocubes were subsequently cast onto hydrophilic substrates, wherein the cubes lined up face-to-face and formed a variety of polygons due to magnetostatic and hydrophobic interactions. The generated surfaces consist primarily of three- and four-sided nanogons; polygons ranging from two to six sides were also observed. Further examination of the nanogons showed that the constraints of the face-to-face assembly of nanocubes often led to bowed sides, strained cube geometries, and mismatches at the acute angle vertices. Additionally, extra nanocubes were often present at the vertices, suggesting the presence of external magnetostatic fields at the polygon corners. These nanogons are inimitable nanoscale magnetic structures with potential applications in the areas of magnetic memory storage and high-frequency magnetics.

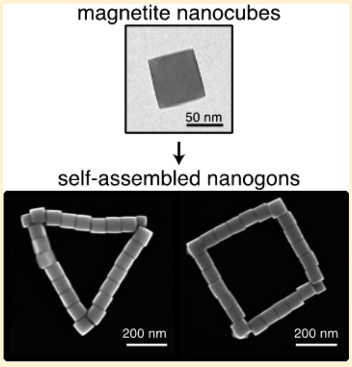

SECTION: Physical Processes in Nanomaterials and Nanostructures

The controlled synthesis and subsequent assembly of magnetic nanomaterials with specific size, shape, and arrangement are essential steps in the fabrication of novel nanostructured devices with unique magnetic properties. Well-defined nanoscale magnetic structures have potential applications in the areas of high-density magnetic energy storage,[1,2] high-frequency electronics,[3,4] photonics,[5] biosensors,[6−8] biomedical therapeutics,[9−11] and separations.[12−14] One particularly useful nanoscale structure that has been suggested for high-density magnetic energy storage devices is a flux-closure ring, a toroidal structure fabricated from ferromagnetic or ferrimagnetic materials that confines the magnetostatic fields inside of the annulus and exhibits unique zero-moment vortex states.[15,16] In short, magnetization runs around the ring, either counterclockwise or clockwise, and can be used as bits (0 or 1, respectively) in memory storage. Flux-closure rings have been created from a range of magnetic materials (Fe, Co, Ni−Fe, Ni−Co, and Fe_3O_4) by top-down nanofabrication techniques including electron beam lithography[16−21] and by deposition over a template coupled with ion beam etching.[22−24] In addition to toroids, other shapes such as nanoscale triangles, squares, and rectangles have been formed by electron beam lithography as flux-closure rings; these geometries have a more complex vortex state structure with additional stable states that has potential application for high-density magnetic storage.[17,21] Solution-based methods offer another route to generation of flux-closure rings by the self-assembly of magnetic nanoparticles.[25−30] These rings typically have a circular structure and significant spacing between the nanoparticles. For example, flux closure rings have been recently prepared using randomly oriented magnetic nanocubes modified with a polyvinylpyrrolidone (PVP) polymer.[30]

In this Letter, we describe the synthesis and face-to-face self-assembly of well-defined nanoscale flux-closure polygons (nanogons) created from uniform magnetite (Fe_3O_4) nanocubes. We are able to generate nanogons of various shapes including triangles, squares, rectangles, trapezoids, and pentagons. These distinctive nanoscale structures arise from a combination of magnetostatic and hydrophobic interactions and only form when the hydrophobic nanocubes are cast onto hydrophilic surfaces. The use of nanocubes leads to the creation of strained angles at the vertices of the nanogons; these strained angles are typically compensated for by a slight curvature in the sides of the polygons. These nanogons are the first examples of nontoroidal nanocube flux-closure rings with well-defined geometries and an internal area in which the self-assembled nanocube building blocks are primarily packed face-to-face. We believe that the formation of these polygonal structures offers a promising route for the fabrication of nanostructured magnetic materials with uniquely tunable shapes and novel magnetic properties.

Uniform magnetite cubes were first synthesized in the presence of oleic acid using a modification of the procedure described by Kim et al.[13] Iron(III) acetylacetonate (0.706 g, 2.00 mmol), oleic acid (1.27 mL, 5.00 mmol), and benzyl ether (10 mL) were heated together to reflux for 30 min. The primary modification to this procedure was to minimize the exposure of the solution to magnetic fields (no magnetic stir bars were used). After refluxing, the solution was cooled to room temperature, washed, and redispersed in chloroform (or

Received: July 12, 2012
Accepted: August 8, 2012

   dx.doi.org/10.1021/jz300931s | J. Phys. Chem. Lett. 2012, 3, 2320−2325

left to dry overnight for the case of the magnetic characterization measurements).

The synthesized cubes were characterized with a combination of electron microscopy (SEM and TEM), selected area electron diffraction (SAED), and X-ray diffraction (XRD) measurements. Figure 1 shows representative SEM and TEM

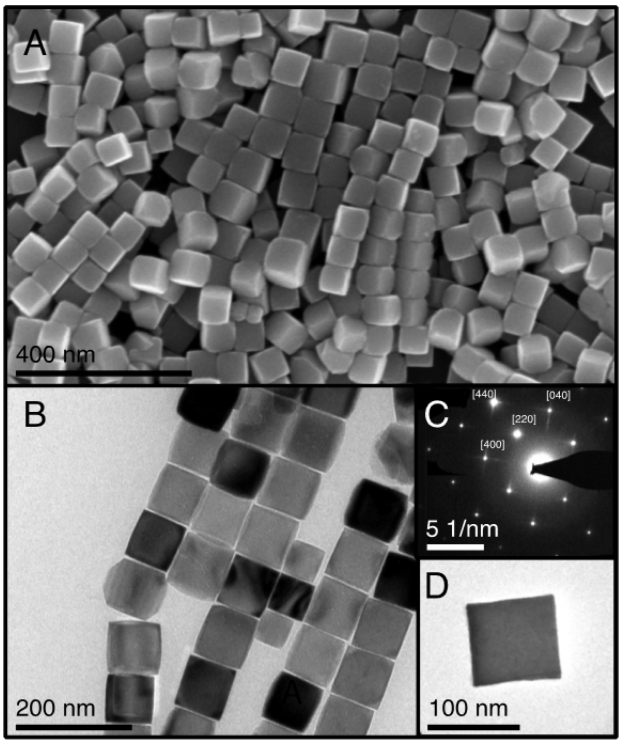

Figure 1. Electron microscopy of synthesized nanocubes. (A) High-resolution SEM image. (B) TEM image. (C) SAED pattern of a single cube. (D) TEM image of the single cube used for SAED.

images of the as-prepared cubes (Figure 1A and B, respectively), demonstrating their uniformity in size and shape. The size distribution estimated by image analysis was found to be 86.3 ± 13.4 nm. SAED of a single magnetite cube is shown in Figure 1C along with a TEM image of the cube from which the SAED pattern was acquired in Figure 1D. The SAED pattern confirms that the nanocubes are single crystals with (100) faces that can be indexed to the inverse spinel, magnetite (JCPDS, 00-019-0629) with space group *Fd*3*m*. Additional XRD measurements were also performed (see Supporting Information, Figure S1) on the as-synthesized nanocubes; the XRD exhibited a set of sharp peaks that were used to confirm the size distribution and crystallinity of the magnetite nanocubes.

Magnetization curves of the magnetite nanocubes were obtained using a vibrating sample magnetometer (SQUID-VSM) and are shown in Figure 2. The data show a saturation value (M_s) of 88 emu/g, which is close to that reported for bulk magnetite (92 emu/g).[31] From this saturation value, the average magnetic dipole value for a nanocube of 2.93×10^{-13} emu was calculated. The magnetic properties of the nanocubes at low applied fields are particularly crucial to the understanding of nanogon assembly and are shown in more detail in an inset to Figure 2. A coercivity value (H_c) of 77 Oe is observed, which is similar to that reported for other magnetite nanocubes.[13] A magnetic remanence value (M_r) of 15.2 emu/g

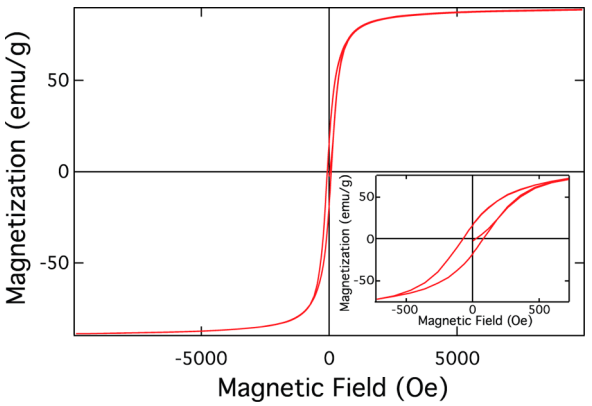

Figure 2. VSM data of the as-synthesized nanocubes. The saturation value (M_s) is 88 emu/g, and the cubes have a coercivity of 77 Oe. The inset shows the low-field curve and suggests that the cubes start close to zero magnetization and get magnetized for the first time in the VSM.

was calculated from the magnetization curves, resulting in a ratio M_r/M_s of 0.17. Various previous studies have reported that the single to multidomain transition size for magnetite nanoparticles is in the range of 54−128 nm;[13,30,32] We deem the 85 nm nanocubes to be "pseudosingle domain" magnets as they fall in the range where the coercivity is observed to increase with size.[13] It is important to recognize that unlike smaller magnetite nanocubes (<20 nm), these nanocubes have a finite coercivity value that renders them weakly ferrimagnetic.[13,33−36] Ferrimagnetic nanocubes can retain a magnetic moment and interact with one another in solution and on surfaces; these interactions are integral to the self-assembly of the flux-closure nanogons. Additionally, because these nanocubes are made of magnetite, face-to-face assembly along the hard [100] axis implies that magnetostatic interactions dominate over the effects of the magnetocrystalline anisotropy.[32] This face-to-face assembly ensures that the flux lines are within the ring itself to allow formation of a vortex state.

Flux-closure nanogons were prepared by the deposition of as-synthesized nanocubes onto hydrophilic surfaces from a chloroform solution. The cubes were synthesized with an oleic acid shell that rendered them hydrophobic and relatively stable in chloroform. Nanocube concentrations ranging from 0.1 to 4.0 mg/mL generated nanogons on both Si and SiO_2 hydrophilic substrates that were prepared by oxygen plasma cleaning. The solution of nanocubes was either drop-cast or spin-coated (1000 rpm, 15 s) onto the substrate. Both procedures generated surfaces with approximately 65% of the objects being nanogons for a nanocube concentration of 2.0 mg/mL (see Supporting Information Figure S2 for a wide-angle SEM image). Nanogons were only observed when there was minimal exposure to magnetic fields during the nanocube synthesis and the substrate was hydrophilic. In control experiments, the hydrophobic nanocubes were also cast onto a hydrophobic substrates formed by surface modification with the organosiloxane SigmaCote. In all cases with hydrophobic substrates, both spin-coated and drop-cast, the nanocubes did *not* form polygons but instead formed aggregates of nanocubes (see Figure S3 in the Supporting Information). This result strongly suggests that the additional hydrophobic interactions of the nanocube surfaces played an important role in the generation of nanogons. Although previous researchers have demonstrated that in some cases, solvent effects can lead to

dx.doi.org/10.1021/jz300931s | *J. Phys. Chem. Lett.* 2012, 3, 2320−2325

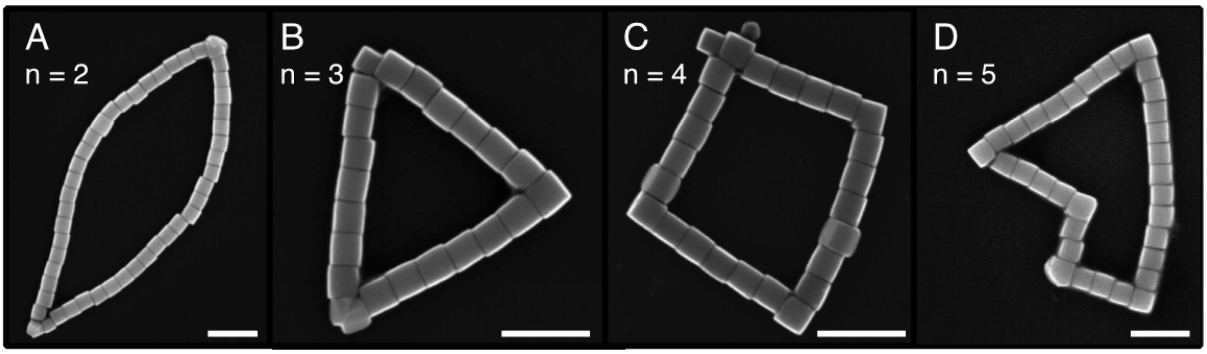

Figure 3. Representative SEM images of nanogons formed from magnetite nanocubes; n = (A) 2, (B) 3, (C) 4, and (D) 5 polygons showing the face-to-face packing in addition to the edge and vertex effects. All scale bars are 200 nm.

flux-closure ring formation, we believe that it is not playing a major role in our nanogon formation for several reasons: (1) As a control similar to work done by Xiong et al.,[30] nanocubes were dispersed in methylene chloride, which has a higher vapor pressure, and nanogons formed on the plasma-cleaned surface. (2) In contrast to previous reports,[37] the surface was not entirely composed of ring structures from solvent evaporation. (3) Ring structures driven by solvent physics often produce larger rings with multiple layers of nanoparticles,[30,37−39] which is not observed in our case. (4) The close face-to-face assembly is indicative of dipolar interactions.[39] From these results, we conclude that it requires a combination of magnetostatic and hydrophobic surface interactions to assemble the nanocubes in a face-to-face manner and generate specific polygonal shapes.

A set of representative nanogons with n sides where n = 2−5 are shown in Figure 3. In all instances, the nanocubes have lined up face-to-face along the [100] direction to form closed loop structures, suggesting that magnetostatic interactions are involved in the self-assembly process. In previous flux-closure ring systems, the nanoparticles are either spherical[25,26,28,29] or do not assemble in this face-to-face manner.[30] Table 1 lists the numbers of different nanogons that we have observed; nanogons with n = 3 or 4 (nanotriangles and nanoquadrilaterals) are the most prevalent shapes. A small number of nanogons with n = 5 or 6 was observed, and an even smaller number of "two-sided" nanogons (n = 2), such as the structure shown in Figure 3A, was seen. We also observed a number of "double line" structures that could potentially exhibit flux-closure vortex states but did not include them in our polygon count as they have two sides but no internal area. Figure 4 shows additional SEM images of the two most common nanogons formed on the surface, n = 3 and 4. These additional figures show that a variety of polygons are present on the surface and that all of the polygons exhibited some imperfections.

Table 1. Analysis of Self-Assembled Nanogons

	no. of total nanogons	% of total nanogons	nanocubes per polygon
n = 2	5	1.0	36.0 ± 15.5
n = 3	233	32.3	18.6 ± 6.6
n = 4	439	60.7	15.6 ± 6.9
n = 5	31	4.5	22.6 ± 8.7
n = 6	10	1.6	22.8 ± 5.3

For the n = 3 nanotriangles, it is clear from Figure 4A−C that the formation of polygon vertices from nanocubes can lead to a significant amount of geometric strain. Nanocube vertices must be 90°, and three 90° nanocube vertices lead to a total of 270° of internal angle as compared to the 180° required for formation of a nanotriangle. This angle strain was typically relieved by a curvature in the polygon side, as seen in Figure 4B and C. This curvature of the polygon sides was also observed in two-sided polygons, as seen in Figure 3A, where the face-to-face nanocube assembly must curve in order to meet at the two vertices. In contrast, the n = 4 polygons have 90° of internal angle per vertex and thus exhibit much less angle strain or polygon side curvature, as seen for the nanorectangles in Figure 4D and E. The larger polygons (n > 4; e.g., Figure 3D) and trapezoids (e.g., Figure 4F) display a combination of right angles and other (acute or obtuse) angles with some angle strain and curvature along the edges.

The average sizes of the various nanogons in terms of the total number of nanocubes are compiled in Table 1. These numbers also show evidence of the internal angle strain in that the nanogons with n = 2 have the largest average number and nanogons with n = 4 have the smallest average number. This trend is appropriate because the internal angle strain is largest for n = 2 and smallest for n = 4. For n = 5 and 6, the average size increases as compared to n = 4 both for internal strain constraints and also simply because a larger number of sides requires more nanocubes.

Further analysis of the SEM images in Figure 4 of n = 3 and 4 nanogons points to the presence of additional magnetostatic fields at the nanogon vertices. In almost all of the nanogons shown in Figure 4, there are additional nanocubes at a vertex. We hypothesize that there are fringing magnetic fields at the vertices that result in the presence of these additional nanocubes. Previous measurements and calculations have shown that nontoroidal flux-closure rings have vortex states with fringing magnetostatic fields at the vertices,[21] and a recent simulation of the self-assembly of nanocubes with nonzero electric dipoles into polygons also shows similar vertex structures.[40]

In summary, the self-assembly of nanoscale flux-closure polygons (nanogons) from magnetite nanocubes offers a novel and potentially powerful route to the formation of distinctive magnetic structures with unique nanoscale electromagnetic properties. We have described herein a self-assembly process of nanogons that occurs when monodisperse magnetite nanocubes are synthesized and then cast onto hydrophilic substrates. The magnetite cubes are single-crystalline, uniform, and ferrimagnetic based on SEM, TEM, SAED, and VSM characterization measurements. The nanocubes assemble face-

dx.doi.org/10.1021/jz300931s | J. Phys. Chem. Lett. 2012, 3, 2320−2325

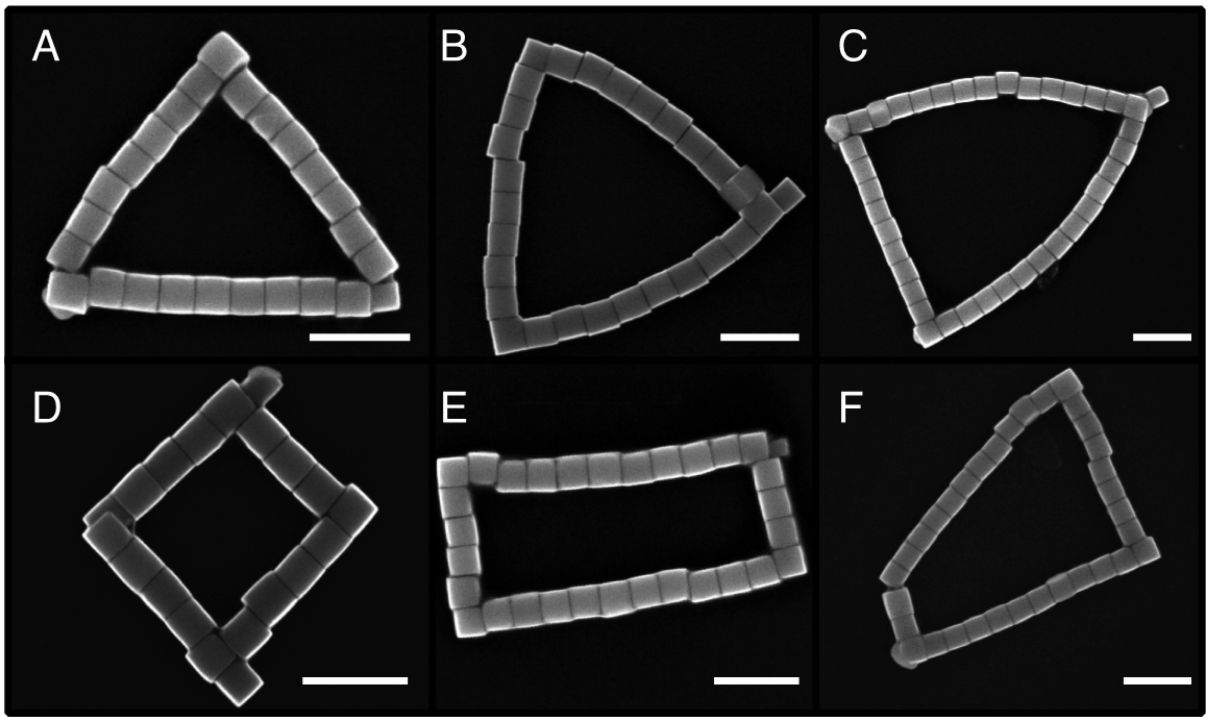

Figure 4. SEM images of a variety of $n = 3$ (A–C) and $n = 4$ (D–F) sided polygons. (A) A 90° isosceles triangle, (B) strained equilateral triangle, (C) strained isosceles triangle with an additional cube at the apex, (D) rectangle (almost square), (E) rectangle, and (F) trapezoid. All scale bars are 200 nm.

to-face primarily into three-sided and four-sided nanogons, but we have also observed two-, five-, and six-sided polygons. Angle strain at a nanogon vertex is compensated for by a slight curvature of the adjacent nanogon sides. Additionally, extra cubes that indicate the presence of fringing magnetostatic fields are frequently attached at the nanogon vertices. Future work will include learning about the magnetostatic fields and dipoles that allow these nanogons to form and determining if they have the interesting vortex magnetic states for nontoroidal geometries that have been both predicted theoretically and observed experimentally with magnetic force microscopy (MFM).[17,21] We also intend to expand the nanogon self-assembly process to patterned hydrophobic substrates in order to better control nanogon formation and generate ordered nanogon arrays.[41,42] We anticipate biofunctionalizing the surface of the nanocubes as we have done previously with Au and Si nanoparticles[43−45] and then using hybridization-directed assembly onto patterned nucleic acid surfaces in order to create patterned nanocube arrays.[46−49]

EXPERIMENTAL METHODS

Synthesis of Magnetite Nanocubes. All chemicals were purchased from Sigma-Aldrich. The magnetite nanocubes were synthesized by modification of literature procedures.[13] Briefly, a three-neck round-bottom flask was charged with iron(III) acetylacetonate (0.706 mg, 2.00 mmol), oleic acid (1.268 mL, 5.000 mmol), and benzyl ether (10 mL). The key modification to the procedure was performing the reaction *without* a magnetic stir bar, using boiling chips instead. Cubes synthesized with a magnetic stir bar served as a control (see Supporting Information Figure S4). The flask was fitted with a thermocouple, and the mixture was subsequently heated to 290 °C for 30 min. The heating mantle was removed immediately, and the solution was allowed to cool to room temperature in air. The mixture was rinsed with a toluene/hexane mixture (4:1 ratio, 30 mL) and centrifuged at 250*g* for 10 min. The black precipitate was washed (2×) with chloroform (30 mL) and centrifuged at 250*g* for 10 min. The final black pellet was suspended in 10 mL of chloroform (or left to dry overnight for magnetic measurements).

Self-Assembly of Nanogons. Silicon wafers and glass slides were cleaned with O_2 plasma prior to using. Solutions of the nanocubes were left to sit at room temperature for a minimum of 1 h in order to allow the large aggregates to fall out of solution. The solutions of the nanocubes (2 μL in $CHCl_3$) were dropped onto the substrate and left to evaporate. Spin-coating was also used to generate nanogons. A solution of nanocubes (50 μL in $CHCl_3$) was spun at 1000 rpm for 15 s. Concentrations of nanocubes ranging from 0.1 to 4.0 mg/mL all produced nanogons by both spin-coating and drop-casting. Spin-coated samples were more uniform, and the density of nanogons decreased with concentration.

Characterization Methods. Transmission electron micrographs and electron diffraction images were obtained using a conventional FEI/Philips CM-20 at 200 kV. Scanning electron microscopy was performed on an FEI Magellan. Magnetic properties were measured by vibrating sample magnetometry using a Quantum Design MPMS SQUID-VSM. Magnetic fields were only scanned in a range of −10 000 Oe (−1T) to 10 000 Oe (1T) as the materials reached saturation well below this limit. The magnetization saturation value (M_s) was taken at 10 000 Oe. The coercivity value (H_c) was calculated as the average of the two values for H when $M = 0$ in the hysteresis curve, while the remanence (M_r) was the intercept at $H = 0$. Powder X-ray diffraction patterns were acquired on a Rigaku Ultima III diffractometer with graphite monochromatized Cu Kα radiation (λ = 1.54178 Å).

■ ASSOCIATED CONTENT

Supporting Information

X-ray diffraction (XRD), wide-angle SEM image of the nanogon surface, SEM image comparing the hydrophobic and hydrophilic surfaces, and SEM image comparing the surface formed from nanocubes synthesized with and without magnetic stir bar (Figures S1−S4). This material is available free of charge via the Internet at http://pubs.acs.org.

■ AUTHOR INFORMATION

Corresponding Author

*E-mail: rcorn@uci.edu.

Notes

The authors declare no competing financial interest.

■ ACKNOWLEDGMENTS

This work is supported by the National Science Foundation, Grant CHE-1057638. The authors would like to thank Prof. Zachary Fisk and Ted Grant for the use of the MPMS SQUID-VSM and would also like to acknowledge UCI-LEXI for both electron microscopy and X-ray facilities. The authors express their gratitude to Aaron R. Halpern at UCI and Prof. Robert W. Erickson at the Univ. of Colorado for their useful scientific discussions.

■ REFERENCES

(1) Sun, S. H. Recent Advances in Chemical Synthesis, Self-Assembly, and Applications of FePt Nanoparticles. *Adv. Mater.* **2006**, *18*, 393−403.

(2) Zeng, H.; Li, J.; Liu, J. P.; Wang, Z. L.; Sun, S. H. Exchange-Coupled Nanocomposite Magnets by Nanoparticle Self-Assembly. *Nature* **2002**, *420*, 395−398.

(3) Lu, S.; Sun, Y.; Goldbeck, M.; Zimmanck, D. R.; Sullivan, C. R. 30-MHz Power Inductor Using Nano-Granular Magnetic Material. In IEEE Power Electronics Conference, Taipei, Taiwan, Nov 5−8, 2007; Institute of Electrical and Electronics Engineers, Inc.: Piscataway, NJ, 2007; pp 1773−1776.

(4) Naughton, B. T.; Majewski, P.; Clarke, D. R. Magnetic Properties of Nickel−Zinc Ferrite Toroids Prepared from Nanoparticles. *J. Am. Ceram. Soc.* **2007**, *90*, 3547−3553.

(5) He, L.; Wang, M.; Ge, J.; Yin, Y. Magnetic Assembly Route to Colloidal Responsive Photonic Nanostructures. *Acc. Chem. Res.* **2012**, DOI: 10.1021/ar200276t.

(6) Wang, J. L.; Munir, A.; Zhu, Z. Z.; Zhou, H. S. Magnetic Nanoparticle Enhanced Surface Plasmon Resonance Sensing and Its Application for the Ultrasensitive Detection of Magnetic Nanoparticle-Enriched Small Molecules. *Anal. Chem.* **2010**, *82*, 6782−6789.

(7) Wang, Y.; Dostalek, J.; Knoll, W. Magnetic Nanoparticle-Enhanced Biosensor Based on Grating-Coupled Surface Plasmon Resonance. *Anal. Chem.* **2011**, *83*, 6202−6207.

(8) Gole, A.; Stone, J. W.; Gemmill, W. R.; zur Loye, H. C.; Murphy, C. J. Iron Oxide Coated Gold Nanorods: Synthesis, Characterization, and Magnetic Manipulation. *Langmuir* **2008**, *24*, 6232−6237.

(9) Neamtu, J.; Verga, N. Magnetic Nanoparticles for Magneto-Resonance Imaging and Targeted Drug Delivery. *Dig. J. Nanomater. Biostruct.* **2011**, *6*, 969−978.

(10) Scarberry, K. E.; Dickerson, E. B.; McDonald, J. F.; Zhang, Z. J. Magnetic Nanoparticle−Peptide Conjugates for In Vitro and In Vivo Targeting and Extraction of Cancer Cells. *J. Am. Chem. Soc.* **2008**, *130*, 10258−10262.

(11) Noh, S.-h.; Na, W.; Jang, J.-t.; Lee, J.-H.; Lee, E. J.; Moon, S. H.; Lim, Y.; Shin, J.-S.; Cheon, J. Nanoscale Magnetism Control via Surface and Exchange Anisotropy for Optimized Ferrimagnetic Hysteresis. *Nano Lett.* **2012**, *12*, 3716−3721.

(12) Stephens, J. R.; Beveridge, J. S.; Williams, M. E. Analytical Methods for Separating and Isolating Magnetic Nanoparticles. *Phys. Chem. Chem. Phys.* **2012**, *14*, 3280−3289.

(13) Kim, D.; Lee, N.; Park, M.; Kim, B. H.; An, K.; Hyeon, T. Synthesis of Uniform Ferrimagnetic Magnetite Nanocubes. *J. Am. Chem. Soc.* **2009**, *131*, 454−455.

(14) Laurent, S.; Forge, D.; Port, M.; Roch, A.; Robic, C.; Elst, L. V.; Muller, R. N. Magnetic Iron Oxide Nanoparticles: Synthesis, Stabilization, Vectorization, Physicochemical Characterizations, and Biological Applications. *Chem. Rev.* **2008**, *108*, 2064−2110.

(15) Zhu, J. G.; Zheng, Y. F.; Prinz, G. A. Ultrahigh Density Vertical Magnetoresistive Random Access Memory. *J. Appl. Phys.* **2000**, *87*, 6668−6673.

(16) Castano, F. J.; Ross, C. A.; Frandsen, C.; Eilez, A.; Gil, D.; Smith, H. I.; Redjdal, M.; Humphrey, F. B. Metastable States in Magnetic Nanorings. *Phys. Rev. B* **2003**, *67*, 184425.

(17) Imre, A.; Varga, E.; Ji, L. L.; Ilic, B.; Metlushko, V.; Csaba, G.; Orlov, A.; Bernstein, G. H.; Porod, W. Flux-Closure Magnetic States in Triangular Cobalt Ring Elements. *IEEE Trans. Magn.* **2006**, *42*, 3641−3644.

(18) Li, S. P.; Peyrade, D.; Natali, M.; Lebib, A.; Chen, Y.; Ebels, U.; Buda, L. D.; Ounadjela, K. Flux Closure Structures in Cobalt Rings. *Phys. Rev. Lett.* **2001**, *86*, 1102−1105.

(19) Yoo, Y. G.; Klaui, M.; Vaz, C. A. F.; Heyderman, L. J.; Bland, J. A. C. Switching Field Phase Diagram of Co Nanoring Magnets. *Appl. Phys. Lett.* **2003**, *82*, 2470−2472.

(20) Heyderman, L. J.; David, C.; Klaui, M.; Vaz, C. A. F.; Bland, J. A. C. Nanoscale Ferromagnetic Rings Fabricated by Electron-Beam Lithography. *J. Appl. Phys.* **2003**, *93*, 10011−10013.

(21) Subramani, A.; Geerpuram, D.; Domanowski, A.; Baskaran, V.; Medushko, V. Vortex State in Magnetic Rings. *Physica C* **2004**, *404*, 241−245.

(22) Singh, D. K.; Krotkov, R. V.; Xiang, H. Q.; Xu, T.; Russell, T. P.; Tuominen, M. T. Arrays of Ultrasmall Metal Rings. *Nanotechnology* **2008**, *19*, 245305.

(23) Singh, D. K.; Krotkov, R.; Tuominen, M. T. Magnetic Transitions in Ultra-Small Nanoscopic Magnetic Rings: Theory and Experiments. *Phys. Rev. B* **2009**, *79*, 184409.

(24) Zhu, F. Q.; Fan, D. L.; Zhu, X. C.; Zhu, J. G.; Cammarata, R. C.; Chien, C. L. Ultrahigh-Density Arrays of Ferromagnetic Nanorings on Macroscopic Areas. *Adv. Mater.* **2004**, *16*, 2155−2159.

(25) Ding, W. F.; Li, Z. W.; Zhou, H.; Zhao, B.; Wan, J. G.; Song, F. Q.; Wang, G. H. Tunable Formation of Ferromagnetic Nanoparticle Rings: Experiments and Monte Carlo Simulations. *J. Phys. Chem. C* **2012**, *116*, 10805−10813.

(26) Hu, M. J.; Lu, Y.; Zhang, S.; Guo, S. R.; Lin, B.; Zhang, M.; Yu, S. H. High Yield Synthesis of Bracelet-like Hydrophilic Ni−Co Magnetic Alloy Flux-Closure Nanorings. *J. Am. Chem. Soc.* **2008**, *130*, 11606−11607.

(27) Snoeck, E.; Gatel, C.; Lacroix, L. M.; Blon, T.; Lachaize, S.; Carrey, J.; Respaud, M.; Chaudret, B. Magnetic Configurations of 30 nm Iron Nanocubes Studied by Electron Holography. *Nano Lett.* **2008**, *8*, 4293−4298.

(28) Tripp, S. L.; Dunin-Borkowski, R. E.; Wei, A. Flux Closure in Self-Assembled Cobalt Nanoparticle Rings. *Angew. Chem., Int. Ed.* **2003**, *42*, 5591−5593.

(29) Wei, A.; Tripp, S. L.; Liu, J.; Kasama, T.; Dunin-Borkowski, R. E. Calixarene-Stabilised Cobalt Nanoparticle Rings: Self-Assembly and Collective Magnetic Properties. *Supramol. Chem.* **2009**, *21*, 189−195.

(30) Xiong, Y.; Ye, J.; Gu, X. Y.; Chen, Q. W. Synthesis and Assembly of Magnetite Nanocubes into Flux-Closure Rings. *J. Phys. Chem. C* **2007**, *111*, 6998−7003.

(31) Cullity, B. D.; Graham, C. D. *Introduction to Magnetic Materials*; John Wiley & Sons, Inc.: Hoboken, NJ, 2009.

(32) Dunin-Borkowski, R. E.; McCartney, M. R.; Frankel, R. B.; Bazylinski, D. A.; Posfai, M.; Buseck, P. R. Magnetic Microstructure of Magnetotactic Bacteria by Electron Holography. *Science* **1998**, *282*, 1868−1870.

(33) Mathew, D. S.; Juang, R. S. An Overview of the Structure and Magnetism of Spinel Ferrite Nanoparticles and Their Synthesis in Microemulsions. *Chem. Eng. J.* **2007**, *129*, 51−65.
(34) Kovalenko, M. V.; Bodnarchuk, M. I.; Lechner, R. T.; Hesser, G.; Schaffler, F.; Heiss, W. Fatty Acid Salts as Stabilizers in Size- and Shape-Controlled Nanocrystal Synthesis: The Case of Inverse Spinel Iron Oxide. *J. Am. Chem. Soc.* **2007**, *129*, 6352−6353.
(35) Hayashi, K.; Sakamoto, W.; Yogo, T. Magnetic and Rheological Properties of Monodisperse Fe_3O_4 Nanoparticle/Organic Hybrid. *J. Magn. Magn. Mater.* **2009**, *321*, 450−457.
(36) Roca, A. G.; Morales, M. P.; O'Grady, K.; Serna, C. J. Structural and Magnetic Properties of Uniform Magnetite Nanoparticles Prepared by High Temperature Decomposition of Organic Precursors. *Nanotechnology* **2006**, *17*, 2783−2788.
(37) Khanal, B. P.; Zubarev, E. R. Rings of Nanorods. *Angew. Chem., Int. Ed.* **2007**, *46*, 2195−2198.
(38) Ohara, P. C.; Gelbart, W. M. Interplay between Hole Instability and Nanoparticle Array Formation in Ultrathin Liquid Films. *Langmuir* **1998**, *14*, 3418−3424.
(39) Tripp, S. L.; Pusztay, S. V.; Ribbe, A. E.; Wei, A. Self-Assembly of Cobalt Nanoparticle Rings. *J. Am. Chem. Soc.* **2002**, *124*, 7914−7915.
(40) Zhang, X.; Zhang, Z. L.; Glotzer, S. C. Simulation Study of Dipole-Induced Self-Assembly of Nanocubes. *J. Phys. Chem. C* **2007**, *111*, 4132−4137.
(41) An, L. J.; Li, W.; Nie, Y. R.; Xie, B.; Li, Z. Q.; Zhang, J. H.; Yang, B. Patterned Magnetic Rings Fabricated by Dewetting of Polymer-Coated Magnetite Nanoparticles Solution. *J. Colloid Interface Sci.* **2005**, *288*, 503−507.
(42) Denis, F. A.; Hanarp, P.; Sutherland, D. S.; Dufrene, Y. F. Nanoscale Chemical Patterns Fabricated by Using Colloidal Lithography and Self-Assembled Monolayers. *Langmuir* **2004**, *20*, 9335−9339.
(43) Lee, H. J.; Wark, A. W.; Corn, R. M. Enhanced Bioaffinity Sensing Using Surface Plasmons, Surface Enzyme Reactions, Nanoparticles and Diffraction Gratings. *Analyst* **2008**, *133*, 596−601.
(44) Sendroiu, I. E.; Warner, M. E.; Corn, R. M. Fabrication of Silica-Coated Gold Nanorods Functionalized with DNA for Enhanced Surface Plasmon Resonance Imaging Biosensing Applications. *Langmuir* **2009**, *25*, 11282−11284.
(45) Zhou, W. J.; Halpern, A. R.; Seefeld, T. H.; Corn, R. M. Near Infrared Surface Plasmon Resonance Phase Imaging and Nanoparticle-Enhanced Surface Plasmon Resonance Phase Imaging for Ultrasensitive Protein and DNA Biosensing with Oligonucleotide and Aptamer Microarrays. *Anal. Chem.* **2012**, *84*, 440−445.
(46) Storhoff, J. J.; Mirkin, C. A. Programmed Materials Synthesis with DNA. *Chem. Rev.* **1999**, *99*, 1849−1862.
(47) Mirkin, C. A.; Letsinger, R. L.; Mucic, R. C.; Storhoff, J. J. A DNA-Based Method for Rationally Assembling Nanoparticles into Macroscopic Materials. *Nature* **1996**, *382*, 607−609.
(48) Gothelf, K. V.; LaBean, T. H. DNA-Programmed Assembly of Nanostructures. *Org. Biomol. Chem.* **2005**, *3*, 4023−4037.
(49) Becerril, H. A.; Woolley, A. T. DNA-Templated Nanofabrication. *Chem. Soc. Rev.* **2009**, *38*, 329−337.